JOURNAL OF GEOPHYSICAL RESEARCH, VOL. 91, NO. C9, PAGES 10,709–10,717, SEPTEMBER 15, 1986

Large-Scale Short-Period Sea Ice Atmosphere Interaction

ROBERT F. CAHALAN

Laboratory for Atmospheres, NASA Goddard Space Flight Center, Greenbelt, Maryland

LONG S. CHIU

Applied Research Corporation, Landover, Maryland
Laboratory for Atmospheres, NASA Goddard Space Flight Center, Greenbelt, Maryland

Changes in the microwave brightness temperature measured by the Electrically Scanning Microwave Radiometer (ESMR) flown on board the Nimbus V satellite reveal large-scale sea ice fluctuations in the Antarctic marginal ice zone. These ice margin fluctuations are predominantly wave numbers 1–4, with phase speeds of about 3 m/s independent of wave number. The spatial pattern and eastward advection of the sea ice anomalies match those of the atmospheric sea level pressure, and are consistent with sea ice displacement due to surface wind stress. Examination of the outgoing longwave radiation indicates that suppression of high clouds in regions of increased sea ice increases the radiative cooling which contributes to maintaining the ice. Data from three winter seasons indicate about a one-third probability of occurence of this large scale high frequency sea ice atmosphere interaction during any given 2-week period in winter.

1. INTRODUCTION

Sea ice is an important climatic variable. Interacting with both atmosphere and ocean, it displays both the long time scales of adjustment associated with the ocean as well as the more rapid changes characteristic of the atmosphere. (For a thorough review, see *Polar Group* [1980]). While much attention has been devoted to monthly and longer time scales, relatively few studies have focused on sea ice variability on the daily time scale. (Exceptions are *Raynor and Howarth* [1979] and *Cavalieri and Parkinson* [1981]). The purpose of this paper is to show that synoptic-scale sea ice fluctuations occur in the region of the sea ice margin, and that their wave numbers and advection speeds suggest a rapid response to synoptic-scale forcing by the atmosphere.

High-frequency synoptic-scale sea ice fluctuations are significant not only because they provide direct evidence of the link with atmospheric variations occurring on the same space and time scales, but also because they represent the primary background of "climatic noise" from which any true climatic signal" must be extracted. In the absence of any true climatic change, the monthly mean sea ice would still exhibit variations due to the integrated effect of the high-frequency changes studied here, much like the drift of a particle experiencing Brownian motion in the absence of any external force. (For applications of this idea to sea ice, see for example *Lemke et al.* [1980] and *Colony and Thorndike* [1985]).

Trends of sea ice extent in the northern hemisphere have been examined by many, notably *Walsh and Johnson* [1979] and *Zakharov and Strokina* [1978]. In the southern hemisphere, sea ice observations have been fragmentary until the advent of satellites which provide a global coverage of the ice field. *Kukla et al.* [1977] have compiled total snow and ice data for the globe. They found that in the southern hemisphere the ice extent in November, which parallels the annual mean ice extent, showed an increase for the period 1966–1972. From 1973–1980, when satellite data were incorporated into the ice analysis, the total Antarctic sea ice area showed a decrease [*Kukla and Gavin*, 1983]. This decrease, amounting to 2.5 million km^2 over the 8-year period, compared to an annual amplitude of 15 million km^2, has caused concern over the possibility of a climatic change. *Zwally et al.* [1983*b*] pointed out that the apparent change may be due to the existence of polynyas in some of the years. *Chiu* [1983] and *Zwally et al.* [1983*b*] extended the time series of the Antarctic sea ice to the middle of 1982 and found that the Antarctic sea ice area rebounded after 1980 to above average values in 1981. Because the downward trend of the mid and late 1970s has not been maintained, a climatic change has yet to be demonstrated.

In order to determine the significance of monthly mean sea ice changes such as those discussed above, it is necessary to estimate the natural variability (or "climatic noise") of the mean. This is the variability which would occur in the absence of any climate change, due only to the finite number of independent samples in the averaging period. The variance of the mean is approximately the variance associated with each sample divided by the number of independent samples. A more careful estimate involves the space-time autocorrelation function, given by

$$\Gamma(p1, p2; \tau) = \overline{\delta C(p1, t)\, \delta C(p2, t + \tau)}/(\sigma_1 \sigma_2)$$

where $\delta C(p, t)$ represents the anomaly in the sea ice concentration at a point p and at a time t, from which the mean seasonal cycle as well as any long term trends have been removed. σ_1 and σ_2 are the standard deviations of δC at $p1$ and $p2$, respectively, and the overbar indicates a seasonal average. *Lemke et al.* [1981] estimated this quantity using weekly data averaged over 10 degree longitudinal sectors. To better interpret their results, higher spatial resolution is clearly desirable, but gaps in the data make it difficult to obtain stable statitics at higher resolution. In this paper we present some case studies which provide a qualitative understanding of the natural variability of sea ice and its correlation with atmospheric forcing.

In the next section we describe the available data. Section 3 describes a difference filter that isolates the high frequency variations, and focuses on one case study of possible sea ice-

Paper number 6C0338.

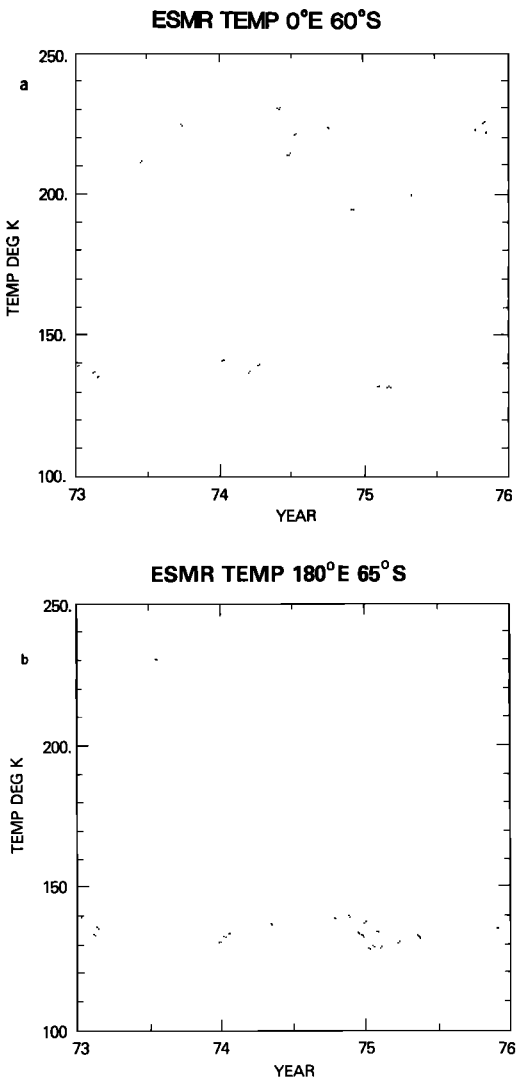

Fig. 1. Time series of 3-day averaged 250-km gridded ESMR brightness temperatures at (*a*) 60 S, 0 E and (*b*) 65 S, 180 E.

atmosphere interaction. Section 4 discusses the various time scales associated with sea ice. Section 5 summarizes our major results, discusses the climatological significance of such sea ice fluctuations, and suggests possible future work in sea ice modeling.

2. The Data

The sea ice data are derived from microwave temperature observations taken on board NIMBUS 5 by the Electrically Scanning Microwave Radiometer (ESMR). A detailed description of both the satellite and the instrument can be found in *Sabatini* [1972]. *Zwally et al.* [1981] describe an algorithm which converts the microwave temperature into ice concentration. Since climatological monthly mean air temperature is used in the algorithm, it may not be appropriate for shorter time scales. Thus our results described in sections 3 and 4 are given in terms of observed brightness temperatures (and their gradients) rather than the derived ice concentrations. In section 4 we show that these brightness variations are dominated by sea ice changes down to periods of 3 to 6 days, at which point other atmospheric and oceanic variables begin to become important.

The data are put on a square polar stereographic map of 293 by 293 grid points, enclosing the 50 S latitude circle and retaining the approximate 30 km resolution of the data. Daily and 3-day averaged values have been computed. The data have also been compressed onto a 41 by 41 grid, having a resolution of about 250 km between grid points.

Monthly averages are also presented in false color mapped format by *Zwally et al.* [1983*a*]. During the period 1973–1976, for which the data are available, there are 7 missing months due to insufficient usable data. For 3-day averages the situation for missing data is worse.

Zwally et al. [1983*a*] have commented on the accuracy of the data. The algorithm for converting brightness temperature to ice concentration is believed to be valid to about 15% of ice concentration in the Antarctic. Because of the strong contrast of emissivity between fresh ice and water at freezing, the edge of the ice is quite distinct. *Rayner and Howarth* [1979] spatially differentiated the brightness temperature and found that the 155 K isotherm lies at the edge of a steep gradient in the field of brightness temperature and corresponds approximately to an ice concentration of 15%. They identified this as the edge of the ice. The same criteria is also used in the work of *Cavalieri and Parkinson* [1981] and *Parkinson and Cavalieri* [1982].

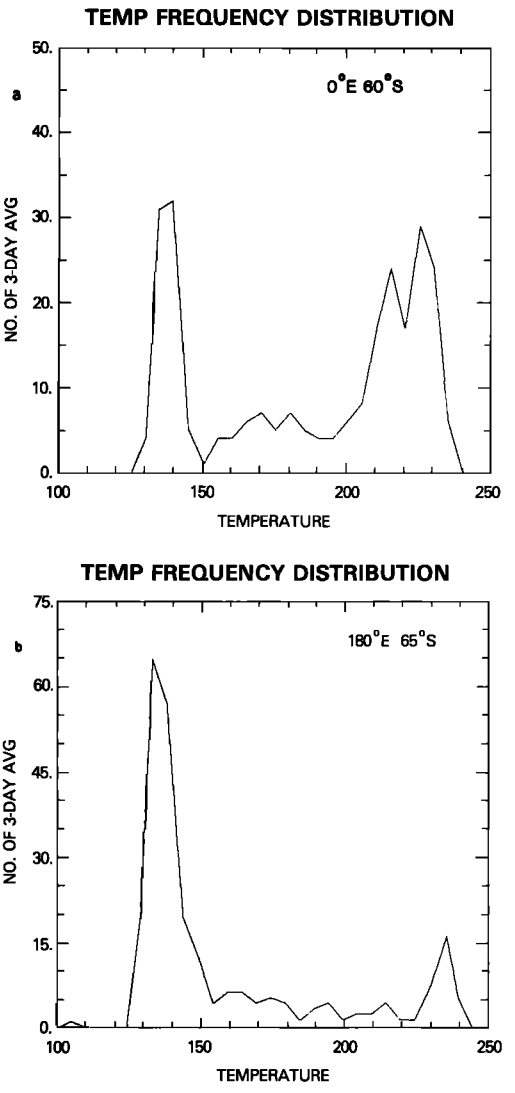

Fig. 2. Histograms of the brightness temperatures from the time series in Figure 1.

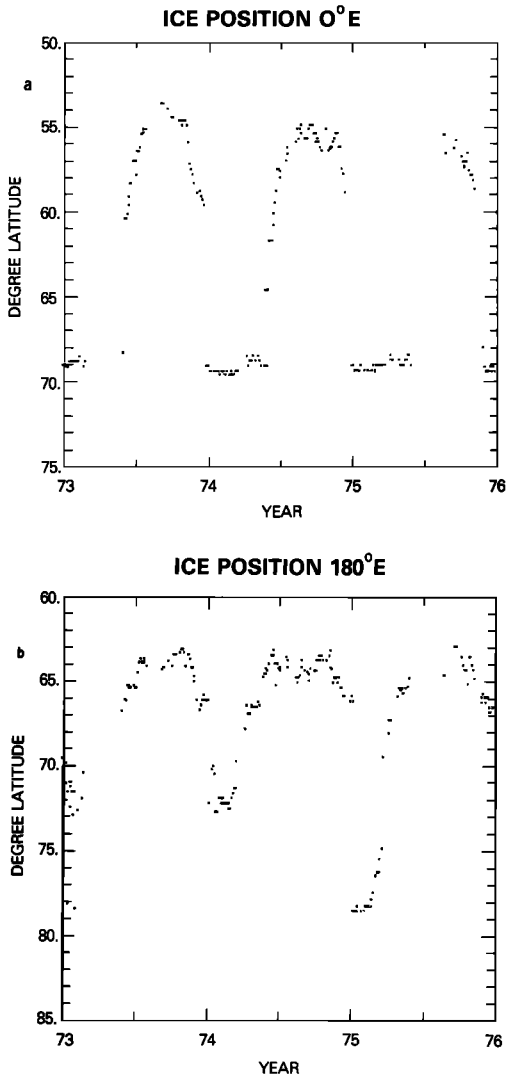

Fig. 3. Time series of the latitudinal position of the ice edge, defined by the 155 K brightness temperature contour (corresponding to about 15% ice concentration) for (*a*) 0 E and (*b*) 180 E.

The atmospheric data used here are the twice daily (11Z and 23Z, but only 23Z before 1974) sea level pressure (SLP) analyses produced by the World Meteorological Center in Melbourne, Australia. This data set is available through the National Center of Atmospheric Research (NCAR). The basic analyses rely on initial specification of mean sea level pressure and 1000 mbar to 500 mbar thickness and incorporate all available conventional and satellite cloud information which give deviations from climatology [*Gauntlett et al.*, 1972]. The quality of the analyses was discussed by *Trenberth* [1979] who made case comparisons between the Australian analyses, the South African hemispheric Analyses, U.S. National Meteorological Center analyses and the regional analyses in New Zealand with observations. He found that "the Australian Analyses are by far the best hemispheric data set available for this period although they contain a few imperfections." From the twice daily data, we computed 3-day averages for our study.

The infrared radiation (IR) data are derived from scanning radiometer measurements aboard the NOAA operational satellites, having atmospheric windows in the 10.5 to 12.5 micron region [see *Gruber and Winston*, 1978]. The data are available twice daily on a 2.5° latitude by 2.5° longitude grid. Again 3-day averages have been computed and used in our study.

3. A Case Study

To see how sea ice affects the ESMR microwave brightness temperature, let us examine two typical time series of 3-day averaged ESMR brightness from grid points at 60 S, 0 E and 68 S, 180 E, shown in Figure 1. These grid points are located in the marginal zones between permanent sea ice and the ocean in the Weddell and Ross seas respectively. Missing data is not plotted. The ocean, at 140 K, is uniformly "cold" in the microwave compared to sea ice, which gives a "hot" signal, as high as 240 K. It can be seen in Figure 1 that the transition from open water, with ESMR brightness temperatures of about 130–140 K, is quite abrupt. The distribution of ESMR temperatures is therefore bimodal, as shown in Figure 2. Figure 3 shows the time series of the ice extent at 0 E and 180 E, which is derived from the brightness temperature using the technique of *Rayner and Howarth* [1979]. One can see the existence of rapid variations of the sea ice extent superposed on the slowly varying seasonal trends.

Figure 4 shows the ice extent as a function of longitude for 3-day averaged data, beginning on Julian day 166 in 1974. For convenience, 3-day averages are denoted by the first day of the 3-day average; e.g., day 166 is the average of day 166–168. Five consecutive 3-day averages are presented, and to clarify the graph each 3-day average is displaced by 3 degrees latitude. Here we see small-scale features embedded in rather irregular large-scale features, and this seasonal pattern shows no evident changes during this two week period. It does, however, change on the seasonal time scale. A Fourier analysis of the seasonal pattern has been described by *Cavalieri and Parkinson* [1981] and *Parkinson and Cavalieri* [1982]. *Comiso and Zwally* [1984] have determined the rate of growth and decay of the seasonal pattern for various longitudinal sectors and months.

3.1. *The Difference Filter*

To focus on the high frequency variations, we shall study only the changes in the microwave brightness temperature

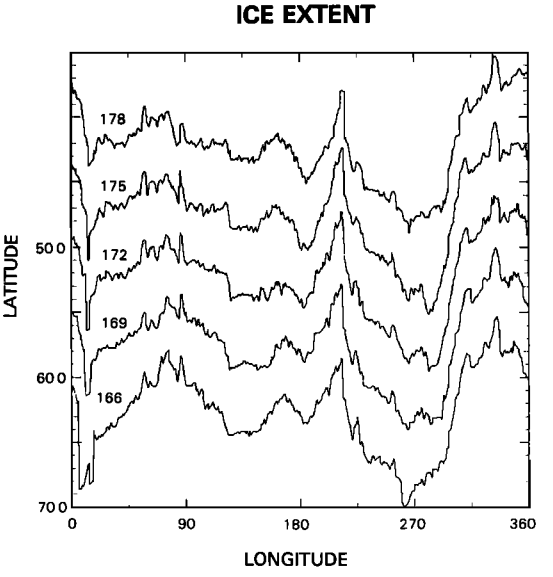

Fig. 4. Three-day averaged ice extent as a function of longitude. Here the curve labelled 166, for example, denotes the average ice extent for days 166–168, 1974. The label on the *y* axis refers to latitude of sea ice extent for day 166–168. Subsequent 3-day averages are offset by 5 degrees latitude for clarity.

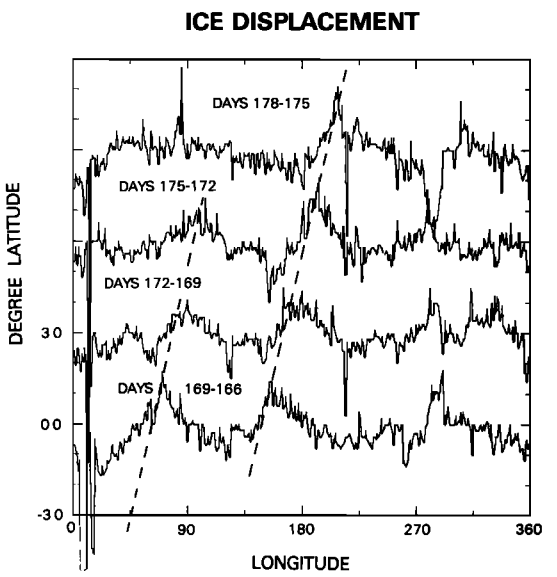

Fig. 5. Change in ice edge position for successive 3-day average ice extents. The label on the y axis refers to ice changes from day 166 to 169 which is labelled 169–166. Subsequent changes are offset by 3 degrees of latitude.

from one time interval to the next, in other words the time derivative. Since the Fourier transform of a time derivative is the Fourier transform weighted by the frequency, the seasonal cycle and other low frequencies are suppressed, and we have a simple high-pass filter. For a more comprehensive discussion on the difference filter, the reader is referred to *Jenkins and Watts* [1975].

The time differencing effectively removes any geographically fixed variations in sea ice extent. It also isolates regions of rapid ice changes with time scales much shorter than the seasonal. This can be understood as follows: Let the extent of sea ice $f(x, t)$ be represented as

$$f(x, t) = m(x, T, t) + f'(x, t)$$

where x, t are longitude and time and $m(x, T, t)$ is a running average over a period of T = one season. Thus m is given by

$$m(x, T, t) = 1/T \int_{t-T/2}^{t+T/2} f(x, t)\, dt$$

and $f'(x, t)$, the residue, represents the rapidly varying component of sea ice variations. Note that $m(x, T, t)$ includes the geographically fixed seasonal pattern previously studied in the literature and evident in Figure 4. Since m is nearly constant during a given week, it can be expanded in a Taylor series about $t = t_0$ of the form

$$m(x, T, t) = m(x, T, t_0) + dm/dt\ (t - t_0)$$

where the first term represents the seasonal mean and the second the seasonal trend within the season. A similar expansion can be obtained for $f'(x, t)$. It can now be seen that the differencing results in

$$f(x, t_2) - f(x, t_1) = (dm/dt + df'/dt)(t_2 - t_1)$$

Note that $m(x, T, t_0)$ is effectively removed by the differencing and what remains is the seasonal trend and intraseasonal fluctuations.

We shall focus on the winter seasons, where the seasonal trend is smaller than the shorter period fluctuations (see for example Figure 1 and Figure 2). Winter is also the season when the so-called "melt pond" effect on the microwave temperature is minimal [see *Zwally et al.*, 1983*a*]. In the following subsection, time differencing is used to reveal the existence of high frequency large-scale sea ice advection which would otherwise be obscure if a high pass filter was not used.

3.2. *High-Frequency Variations*

In order to suppress the seasonal and geographical pattern seen in Figure 4, we take the difference between each successive 3-day average as discussed in the previous subsection. Figure 5 shows the resulting ice extent changes for this period. Days 169–166 denotes ice extent change from the 3-day average of 166 to 169. An increase in ice latitude represents a retreat in the ice line. Large scale anomalies which are moving eastward are now evident, and the peaks on each successive day are connected by dashed lines. From the slope of the dashed lines, an eastward speed of about 2.5 m/s at 60 S is estimated.

A space-time spectral analysis has been performed on the 3-day average ice extent changes for the winters of 1973 and 1974. Winter here is defined as day 153 to 240. A description of the space-time spectral methodology is contained in the appendix. Because the difference between 3-day averages is used, a missing time point in the ice extent data represents 2 missing points in the ice change. The missing data points were not included in the analysis.

Previous studies have shown that large scale features dominate the longitudinal variations of sea ice extent, with zonal harmonics 1–6 explaining about 90% of the zonal variance [*Cavalieri and Parkinson*, 1981]. Much of this variance is due

TABLE 1. Space-Time Spectrum of Ice Changes

		Wave Number					
	Frequency	1	2	3	4	5	6
1973	1	0.10	0.64	1.58	0.92	0.14	0.08
		(−64)	(30)	(78)	(29)	(18)	(82)
	2	0.07	1.17	0.33	0.06	0.13	0.01
		(94)	(87)	(−26)	(9)	(64)	(23)
	3	0.05	0.20	0.43	0.19	0.09	0.01
		(15)	(−67)	(75)	(96)	(66)	(−32)
	4	0.02	0.00	0.65	1.10	0.83	0.07
		(47)	(−7)	(57)	(77)	(93)	(95)
	5	0.04	0.04	0.16	0.58	0.00	0.13
		(92)	(−71)	(83)	(95)	(−12)	(76)
	6	0.03	0.02	0.04	0.11	0.12	0.00
		(−99)	(86)	(−26)	(−25)	(82)	(82)
1974	1	0.33	3.76	9.29	0.00	0.00	0.24
		(−39)	(−38)	(93)	(82)	(25)	(−52)
	2	0.01	0.07	4.11	0.37	0.01	0.24
		(64)	(−60)	(87)	(−81)	(14)	(−42)
	3	0.03	0.04	0.09	3.38	0.17	0.00
		(−73)	(−74)	(−6)	(81)	(−37)	(−67)
	4	0.04	0.46	0.09	0.02	0.01	0.09
		(−9)	(79)	(53)	(76)	(17)	(89)
	5	0.03	0.07	0.01	0.98	0.02	0.01
		(95)	(18)	(−53)	(59)	(26)	(−66)
	6	0.26	0.02	0.01	0.06	0.02	0.14
		(63)	(13)	(56)	(50)	(−17)	(27)

Units are in 0.01 (degree/3 day)^2 for the variance spectrum (upper number) and hundredths (in parenthesis) for the net propagating tendency. The total power in the space-time spectra for 1973 and 1974 is 26.7 and 29.1, respectively, in the same units. The net propagating tendency is defined as positive for a eastward propagating wave. Unit of frequency is cycles/48 days.

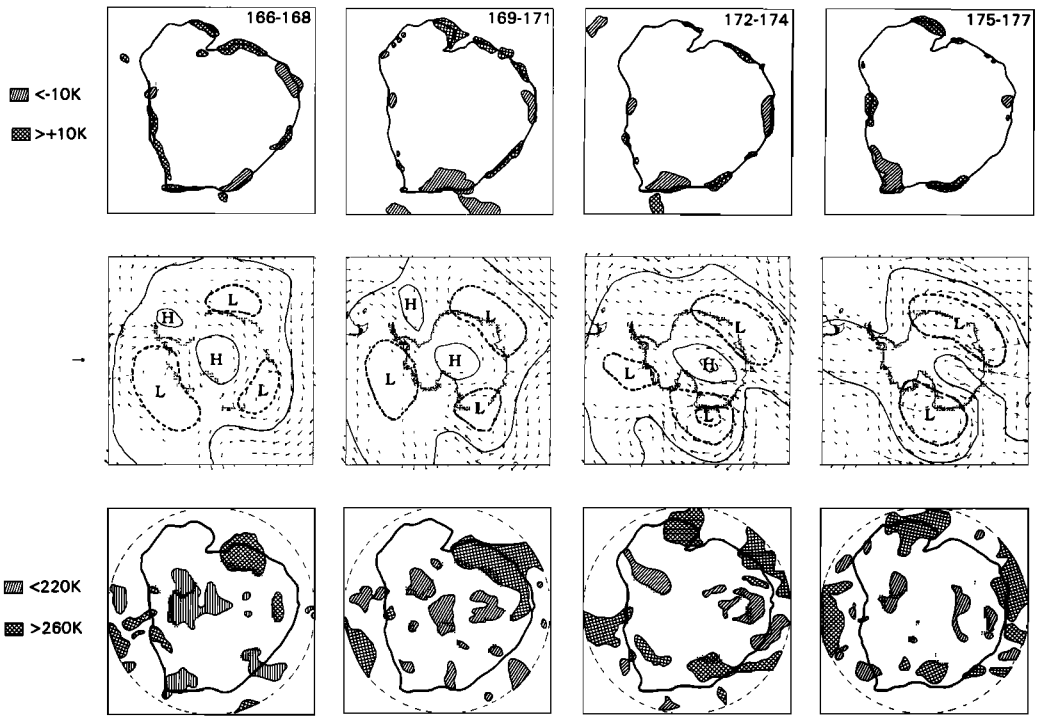

Fig. 6. ESMR temperature changes from the 3-day average indicated on the upper right hand corner of each graph. The 160 K isotherm is included to indicate the approximate position of the ice edge (upper panels). The middle panels show the 3-day average sea-level pressure and surface wind. Solid contours encircle regions of high pressure (> 1008 mbar) and dashed contours encircle regions of low pressure (< 992 mbar). The lower panels show the field of outgoing infrared radiation, derived from radiometric measurements aboard NOAA satellites, with high temperature (> 260 K) stippled and low temperature (< 220 K) shaded.

to the seasonal pattern $m(x, T, t)$ discussed above. In the spectra of ice extent changes, we find that large scale features still dominate, but are less pronounced, with about 50% of the zonal variance contained in the first 6 zonal harmonics.

Table 1 shows the space-time spectrum for planetary wave numbers 1–6. The upper number is the variance in units of 0.01 (degree/3 days)^2, and should be compared with the total variance, 26.7 and 29.1 in 1973 and 1974, respectively. For 1973, the locus of maximum variance is approximately a straight line with lower frequencies corresponding to larger scales on the frequency–wave number plot. The ratio of frequency to wave number, which is the group velocity (here roughly 3 m/s), is independent of wave number, consistent with an advective process. The numbers in parentheses are the net propagating tendencies (see appendix). They show an eastward propagation for wave numbers 3 and 4 (with some low power exceptions). Because of the short duration of the time series and the number of missing data points, this result must be considered tentative and serves merely as a different representation of Figure 5.

The position of the sea ice edge is determined by sea ice advection and melting or freezing. The displacement of the ice edge in turn affects the energy balance of the ice edge and hence there are strong feedbacks between sea ice and atmospheric and oceanic variations. *Lemke et al.* [1981] used a dynamical model which includes lateral diffusion and advection to model Arctic and Antarctic sea ice variations. The data used in their study were weekly mean ice extents for every 10 degrees of longitude for the Antarctic and monthly means with the same spatial resolution for the Arctic. They found that both diffusion and advection are important in explaining sea ice variations in the Antarctic. The advective speeds found in their analysis compare favorably with those of the long term observed ocean currents.

What is the nature of these eastward propagating anomalies found in our case study? The space and time scales are clearly different from those of Lemke et al., though that could be due to the coarser resolution and/or statistical averaging employed in that study. The large scale and the high speed of the propagation observed here suggest an atmospheric connection. *Ackley* [1980] has reviewed various possible interaction mechanisms between sea ice and atmospheric variables. Most of the studies examine the association on time scales from weekly to monthly. One appealing example is the wind driven mechanism proposed by *Gordon and Taylor* [1975] for the seasonal change of the ice cover. Their hypothesis entailed a divergent ice field driven by Ekman drift induced by a divergent wind field. Qualitative agreement between the observed and predicted ice expansion during the period of ice advance of the seasonal cycle was found. On a shorter time scale, *Hibler and Ackley* [1983] did a simulation of the sea ice pack in the Weddell sea with an ice model that included ice dynamics driven by the observed atmospheric conditions. *Thorndike and Colony* [1982] also showed that 50% of the ice motion in the Arctic can be interpreted in terms of the surface geostrophic wind alone. In the following, we shall examine the relation of the ice anomalies and the surface wind as indicated by the sea-level pressure.

The ESMR temperature changes for 3-day averages are shown in Figure 6 for the period of our case (upper panel). The 160 K isotherm is included to indicate the approximate position of the ice edge. A positive change in ESMR temperature represents either an increase in ice concentration or an advance of the ice. Comparing the ESMR brightness temper-

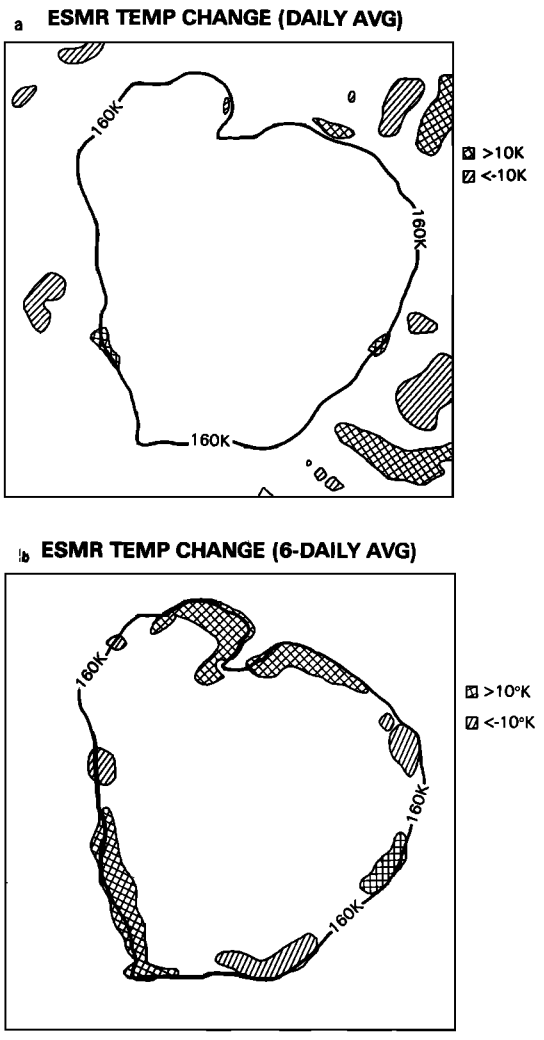

Fig. 7. (*a*) ESMR temperature change between daily averages of days 167 and 166. (*b*) ESMR temperature changes between 6-day average temperatures for periods beginning on days 169 and 163.

ature and the ice extent change, it can be seen that increases in ice extent correspond to increases in ESMR temperature. (Recall that the brightness temperature of ice is considerably higher than that of open water at the wavelength of the ESMR instrument.) The corresponding 3-day averaged sea-level pressure is shown in the middle panel of Figure 6. During this period, the synoptic situation in the Antarctic is characterized by the usual climatological high pressure over the pole, and eastward-moving pressure systems, typically of waves 2–4, along the open water/sea ice boundary. There seems to be a correspondence between the low pressure areas and the regions of ice advance. The eastward speed of the pressure systems is estimated to be roughly 3 m/s, agreeing roughly with the speed of the ice anomalies.

The correspondence between areas of sea ice growth and low pressure centers was also noted by *Cavalieri and Parkinson* [1981] in examining sea ice and circulation changes. They showed a case in which the pressure field is almost stationary, with the trough of zonal wave number 2 in sea level pressure located in the Ross and eastern Weddell sea. There is rapid sea ice growth in the western and central Weddell sea. The suggestion is that the sea ice growth is due to sustained advection of cold air from the more southern latitudes and an equatorward transport of sea ice. The rapid response of the sea ice in our case suggests a dynamic response as opposed to that observed for stationary monthly mean conditions which is probably more thermodynamic in nature.

On the lower panel of Figure 6 is shown the corresponding 3-day averaged infrared radiation (IR) derived from radiometric measurement aboard the NOAA satellites for the same period. Since the effective radiative temperature of clear air is nearly equal to the surface temperature, while in the presence of high clouds it drops to a value near the tropopause, the outgoing IR is a better indicator of high cloud than surface pressure. (See, for example, *Cahalan et al.* [1982], and references therein.) Regions of low IR are generally associated with high cloudiness, except over the high elevations of the continent, where the surface temperature may approach that of the tropopause. Conversely, high IR generally implies low cloudiness. Note that there is no indication of high cloud associated with the low pressure centered at the upper right in the Indian Ocean sector.

While Figure 6 shows no clear correlation between the IR and the ESMR temperature at each point, the positive ESMR anomalies do tend to be associated with high IR. This is consistent with the idea that in regions of increased sea ice concentration, one has reduced evaporation and correspondingly

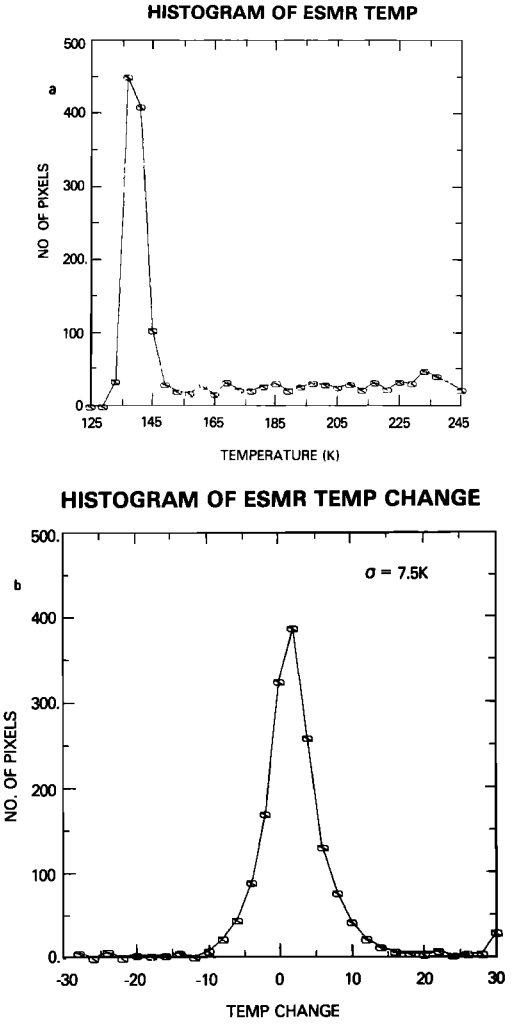

Fig. 8. (*a*) Histogram of 6-day average temperature beginning on day 163. (*b*) Histogram of 6-day average temperature changes between periods beginning on days 169 and 163.

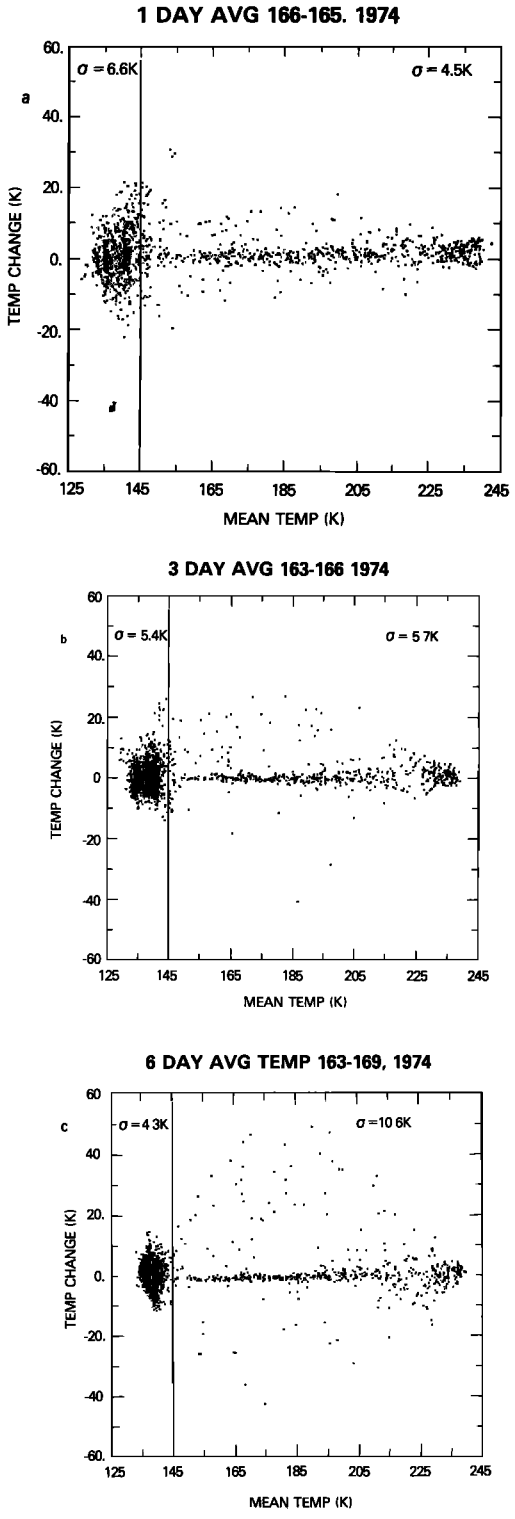

Fig. 9. Scatter diagrams of mean temperature versus temperature changes for (*a*) 1-day, (*b*) 3-day, and (*c*) 6-day averages.

less cloudiness, and thus increased IR cooling to space, which tends to reinforce the formation of sea ice. Such positive feedback between sea ice and cloudiness has been suggested by various investigators [e.g., *Crane and Barry*, 1984; *Carsey*, 1980]. While it certainly cannot be verified with any statistical confidence from the few cases studied so far, these cases do point to an important possible relationship which should be tested in models having interactive cloudiness, once some confidence is gained in the model cloudiness itself.

TABLE 2. Standard Deviations of ESMR Temperature Changes for Different Averaging Periods

Averaging Period	Regime: Water (< 145 K), K/day	Regime: Ice (> 145 K), K/day	Ratio
1 day	6.6	4.5	0.68
3 day	1.8	1.8	1.0
6 day	0.72	1.6	2.2

4. Time Scales

In the case study of section 3, 3-day averaged ice extent is used because it is readily available. The microwave temperature, from which the ice extent is derived, is a function not just of the ice but also of a number of atmospheric and oceanic variables (e.g., water content, surface wind, sea temperature and atmospheric temperature) and therefore contains other time scales associated with these variables. To assess the significance of an ice signal in our case study, an examination of the time scales is in order.

Figure 7 depicts the effect of time averaging on the field of ESMR temperature changes. In Figure 7*a* is shown the temperature change from 1 day (day 165) to the next day. It can be seen that most of the large changes (> 10 K) are located in regions outside the 160 K contour (i.e., over the open ocean). These changes are therefore indicative of meteorological changes over the ocean. Figure 7*b* shows a similar field of ESMR temperature and ESMR temperature changes for 6-day averaged data. It can now be seen that most of the large changes are concentrated along the 160 K contour, indicating an ice signal in the ESMR temperature. Differences as large as 20–30 K are present, but only the 10 K isotherm is indicated for clarity. For 3-day averages (Figure 6) a major fraction of the large changes are found along the 160 K isotherm, but patches are also found over the open ocean. Hence the 3-day averaging period is probably the minimum time scale for sampling ice changes.

The standard deviations of the temperature changes for 6 day averages depicted in Figure 7*b* have been calculated and the histograms of both the temperature and the associated temperature changes are shown in Figure 8. While the histogram of temperature (Figure 8*a*) shows a sharp peak at 135 K and a relatively broad peak at 235 K, representing the water and ice regimes, respectively, the histogram of temperature changes (Figure 8*b*) shows a bell-shaped distribution, with standard deviation of 7.5 K per 6 days, or 1.25 K per day.

To delineate temperature changes due to changes in the ice and water, respectively, Figure 9 shows plots of the temperature changes versus the mean temperature for 1-day, 3-day, and 6-day averages. For 1-day averages (Figure 9*a*) a large scatter is found near 135 K, whereas for 6-day average changes (Figure 9*c*) a large scatter is found at temperatures greater than 145 K.

To quantify the effect of time averaging, the data have been divided into the ice and water regimes and the standard deviations computed for different averaging periods. The results are summarized in Table 2. The ice regime is defined as the region in which the mean temperature exceeds 145 K, and the water regime is defined as the region in which the mean temperature is less than 145 K. From the relation between ice concentration and microwave temperature, the 145 K isotherm corresponds roughly to an ice concentration of 10% [*Zwally et al.*, 1983*a*]. From Table 2 one can see the drastic

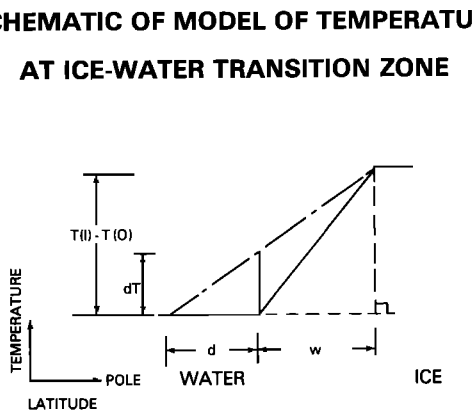

Fig. 10. Schematic of model of temperature at the interface between sea ice and open ocean.

increase in the ratio of the ice regime standard deviation to the water regime standard deviation as the averaging period increases. Thus, as the period increases from 3 days, the ESMR temperature changes are increasingly dominated by the ice regime.

The ice regime can further be divided into a permanent ice zone and a marginal ice zone. The permanent ice zone is characterized by points that show little change, i.e. points located near the x-axis in Figure 9. These points constitute a major portion of the sea ice area, but show no large variability.

The above exercise suggests 3-day averaging is probably the minimum averaging period required for filtering out sufficient meteorological variability, while still retaining the ice signal in the ESMR temperature field.

5. Summary and Discussion

Based on the cases studied here, the following observations have been made of the high-frequency variability of sea ice: wave numbers 1–4 predominate; advective speeds of about 3 m/s; consistent with forcing by surface wind stress; increased ice associated with increased radiative cooling.

From the three winter seasons of data available from ESMR we can obtain some idea of the representativeness of the case study described in section 3. Out of all cases in which at least 5 successive 3-day averages are available during this period, we have found 3 cases similar to Figure 5, in which advecting large-scale sea ice anomalies are evident, and 6 cases in which they are not observed. There is thus about a one-third probability of observing this phenomenon during any given 2-week period in the winter.

In order to relate the observed changes in ESMR brightness temperature to changes in sea ice, we consider a simple model. We imagine a linear profile of temperature at the interface between sea ice and water, decreasing from the sea ice temperature $T(I)$ to the ocean temperature $T(O)$ over a distance of w degrees of latitude, as shown in Figure 10. If the ice edge is then displaced by a distance d, the largest temperature change occurs at the previous location, and is given by

$$\delta T = (T(I) - T(O))d/(d + w)$$

For $T(I) = 235$ K, $T(W) = 135$ K, $w = 2$ degrees latitude, and $d = 0.5$ degrees latitude, this temperature change is about 20 K, consistent with typical values seen in Figure 6. Note that we could shift the ice boundary on the right also, but as long as $d \ll w$ the results are not sensitive to such changes. Larger ice edge displacements presumably require a more realistic nonlinear dynamical model.

Whether the observed temperature anomalies are associated with any displacement of the marginal ice zone, or are due instead to changes in ice concentration within the zone is certainly open to question. While the data appears incapable of resolving this question at present, it would be interesting to see how various sea ice models of Antarctica would respond to planetary-scale pressure waves. The results of such an experiment could be compared with results of the case study presented here, and may also suggest new features of the natural variability of sea ice.

Appendix: Space-Time Spectral Analysis

Hayashi [1971] introduced a method of decomposing a wave field into retrogressive (westward) and progressive (eastward) travelling waves. Let the field of space and time be represented as spatial Fourier components

$$y(x, t) = \sum_k (C_k(t) \cos(kx) + S_k(t) \sin(kx)) \tag{A1}$$

where k is the zonal wave number. Also assume that the seasonal trend and zonal means have been removed, so that

$$\int y\, dt = 0 = \int y\, dx \tag{A2}$$

The coefficients C_k and S_k are determined by multiplying Eq. (A1) by $\cos(kx)$ and $\sin(kx)$, respectively, and integrating over x. If we assume that y consists of travelling waves in the form

$$y(x, t) = \sum_k \sum_j (R_{kj} \cos(kx + jt + \Phi_{kj}) + R_{k-j} \cos(kx - jt + \Phi_{k-j})) \tag{A3}$$

where j is angular frequency, the first term represents westward motion, and the second term represents eastward motion. Expanding (A2) in the form of (A1) and equating coefficients, we get expressions for R_{kj}, R_{k-j}, Φ_{kj}, and Φ_{k-j}. Expanding the coefficients as

$$\begin{aligned} C_k(t) &= \sum_j (A_{kj} \cos(jt) + B_{kj} \sin(jt)) \\ S_k(t) &= \sum_j (a_{kj} \cos(jt) + b_{kj} \sin(jt)) \end{aligned} \tag{A4}$$

then the cross spectral quantities are evaluated as

$$P_j(C_k) = (A^2 + B^2)/2 \qquad P_j(S_k) = (a^2 + b^2)/2$$

$$Q_j(C_k, S_k) = (Ba - Ab)/2 \qquad K_j(C_k, S_k) = (Aa + Bb)/2 \tag{A5}$$

where P is the power spectrum, Q is the quadrature spectrum, and K is the cospectrum. The progressive and retrogressive spectral power is given by

$$\begin{aligned} PE(k, j) &= (P_j(C_k) + P_j(S_k) + 2Q_j(C_k, S_k))/4 \\ PW(k, j) &= (P_j(C_k) + P_j(s_k) - 2Q_j(C_k, S_k))/4 \end{aligned} \tag{A6}$$

respectively.

The net propagating tendency, defined as [*Straus and Shukla*, 1981]:

$$NPT = (PE - PW)/(PE + PW) \tag{A7}$$

is therefore positive if $PE > PW$, i.e., a net eastward propagation.

Acknowledgments. We especially wish to thank D. Cavalieri, C. Parkinson and K. C. Mo for providing us with the data, and for many helpful conversations. We have also benefited from discussions with T. Bell, J. Comiso, P. Gloersen, E. Mollo-Christensen, G. North, and J. Zwally. Finally, both authors wish to thank their coworkers at Goddard for encouraging us through various health problems during the course of this work.

REFERENCES

Ackley, S. F., A review of sea-ice weather relationship in the southern hemisphere: Sea level, ice and climatic changes, *IAHS Publ., 131*, 127–159, 1980.

Cahalan, R. F., D. A. Short, and G. R. North, Cloud fluctuation statistics, *Mon. Weather Rev., 110*, 26–34, 1982.

Carsey, F., Microwave observation of the Weddell Polynya, *Mon. Weather Rev., 110*, 2032–2044, 1980.

Cavalieri, D. J., and C. L. Parkinson, Large-scale variations in observed Antarctic sea ice extent and associated atmospheric circulation, *Mon. Weather Rev., 109*, 2323–2336, 1981.

Chiu, L. S., Variation of Antarctic sea ice: An update, *Mon. Weather Rev., 111*, 478–580, 1983.

Colony, R., and A. S. Thorndike, Sea ice motion as a drunkard's walk, *J. Geophys. Res., 90*, 965–974, 1985.

Comiso, J. C., and H. J. Zwally, Concentration gradients and growth decay characteristics of the seasonal sea ice cover, *J. Geophys. Res., 89*, 8081–8103, 1984.

Crane, R. G., and R. G. Barry, The influence of clouds on climate with a focus on high latitude interactions, *J. Climatol., 4*, 71–93, 1984.

Gauntlett, D. J., R. S. Seaman, W. R. Kininmonth, and J. C. Langford, An operational evaluation of a numerical analysis-prognosis system for the Southern Hemisphere, *Aust. Meteorol. Mag., 20*, 61–82, 1972.

Gordon, A. L., and H. W. Taylor, Seasonal change of Antarctic sea ice, *Science, 187*, 346–347, 1975.

Gruber, A., and J. S. Winston, Earth-atmosphere radiative heating based on NOAA scanning radiometer measurements, *Bull. Am. Meteorol. Soc., 59*, 1570–1573, 1978.

Hayashi, Y., A generalized method of resolving disturbances into progressive and retrogressive waves by space Fourier and time spectral analysis, *J. Meteorol. Soc. Jpn, 49*, 125–128, 1971.

Hibler, W. D., III, and S. F. Ackley, Numerical simulation of the Weddel sea pack ice, *J. Geophys. Res., 88*, 2873–2887, 1983.

Jenkins, G. M., and D. J. Watts, *Spectral Analysis and its Applications.* 525 pp., Holden-Day, San Francisco, Calif., 1975.

Kukla, G. J., and J. Gavin, Summer ice and carbon dioxide, *Science, 214*, 4520, 1983.

Kukla, G. J., J. K. Angell, J. Korshover, H. Dornia, M. Hoshiai, J. Namias, M. Rodewall, R. Yamamoto, and T. Iwashima, New data on climatic trends, *Nature, 270*, 573–580, 1977.

Lemke, P., E. W. Trinkl, and K. Hasselmann, Stochastic dynamic analysis of polar sea ice variability, *J. Phys. Oceanogr., 10*, 2100–2120, 1981.

Parkinson, C. L., and D. J. Cavalieri, Interannual sea-ice variations and sea-ice/atmosphere interactions in the southern ocean, 1973–1975, *Ann. Glaciol., 3*, 249–254, 1982.

Polar Group, Polar atmosphere-ice-ocean processes: A review of polar problem in climate research, *Rev. Geophys., 18*, 525–543, 1980.

Rayner, J. N., and D. A. Howarth, Antarctic sea ice 1972–1975, *Geogr. Rev., 69*, 202–211, 1979.

Sabatini, R. R. (Ed.), NIMBUS 5 user's guide, NASA Goddard Space Flight Cent., Greenbelt, Md., 1972.

Straus, E. M., and J. Shukla, Space-time spectral structure of a GLAS general circulation model and a comparison with observation, *J. Atmos. Sci., 38*, 902–917, 1981.

Thorndike, A. S., and R. Colony, Sea ice motion in response to geostrophic winds, *J. Geophys. Res., 87*, 5845–5852, 1982.

Trenberth, K. E., Interannual variability of the 500 mb zonal mean flow in the southern hemisphere, *Mon. Weather Rev., 107*, 1515–1524, 1979.

Walsh, J. E., and C. M. Johnson, An analysis of sea ice fluctuation 1953–1977, *J. Phys. Oceanogr., 9*, 580–591, 1979.

Zakharov, V. F., and L. A. Strokina, Recent variations in the extent of Arctic Ocean sea ice cover, *Meteorol. Gidrol., 7*, 35–43, 1978.

Zwally, H. J., J. C. Comiso, and C. L. Parkinson, Satellite-derived ice data sets, 1, Antarctic monthly average microwave brightness temperature and sea ice concentrations 1973–1976, *NASA Tech. Memo., TM-83812*, 32 pp., 1981.

Zwally, H. J., J. C. Comiso, C. L. Parkinson, W. J. Campbell, F. D. Carsey, and P. Gloersen, Antarctic sea ice, 1973–1976: Satellite passive-microwave observations, *NASA Spec. Publ., SP-459*, 206 pp., 1983*a*.

Zwally, H. J., C. L. Parkinson, and J. C. Comiso, Variability of Antarctic sea ice and changes in carbon dioxide, *Science, 220*, 1005–1012, 1983*b*.

R. F. Cahalan, Laboratory for Atmospheres, Code 613, NASA Goddard Space Flight Center, Greenbelt, MD 20771.

L. S. Chiu, Applied Research Corporation, Landover, MD 20785.

(Received January 15, 1986;
accepted June 19, 1986.)